Effect of Mono-, Di-, and Triethylene Glycol on the Activity of Phosphate-Doped NiMo/Al$_2$O$_3$ Hydrotreating Catalysts

Alexey L. Nuzhdin [1],*, Galina A. Bukhtiyarova [1,2], Aleksander A. Porsin [1], Igor P. Prosvirin [1], Irina V. Deliy [1,2], Vladimir A. Volodin [2,3], Evgeny Yu. Gerasimov [1,2], Evgeniya N. Vlasova [1,2] and Valerii I. Bukhtiyarov [1,2]

[1] Boreskov Institute of Catalysis SB RAS, 630090 Novosibirsk, Russia; gab@catalysis.ru (G.A.B.); porsin@catalysis.ru (A.A.P.); prosvirin@catalysis.ru (I.P.P.); delij@catalysis.ru (I.V.D.); gerasimov@catalysis.ru (E.Y.G.); evgenia@catalysis.ru (E.N.V.); vib@catalysis.ru (V.I.B.)

[2] Novosibirsk National Research University, 630090 Novosibirsk, Russia; volodin@isp.nsc.ru

[3] Rzhanov Institute of Semiconductor Physics SB RAS, 630090 Novosibirsk, Russia

* Correspondence: anuzhdin@catalysis.ru; Tel.: +7-383-3269-410

Abstract: The effect of glycols on the catalytic properties of phosphate-doped NiMo/Al$_2$O$_3$ catalysts in the hydrotreating of straight-run gas oil (SRGO) was studied. The NiMo(P)/Al$_2$O$_3$ catalysts were prepared using ethylene glycol (EG), diethylene glycol (DEG), and triethylene glycol (TEG) as additives. The organic agent was introduced into the aqueous impregnation solution obtained by the dissolving of MoO$_3$ in H$_3$PO$_4$ solution, followed by Ni(OH)$_2$ addition. The Raman and UV–Vis studies show that the impregnation solution contains diphosphopentamolybdate H$_x$P$_2$Mo$_5$O$_{23}^{(6-x)-}$ and Ni(H$_2$O)$_6^{2+}$, and that these ions are not affected by the presence of glycols. When the impregnation solution comes in contact with the γ-Al$_2$O$_3$ surface, H$_x$P$_2$Mo$_5$O$_{23}^{(6-x)-}$ is decomposed completely. The catalysts were characterized by Raman spectroscopy, low-temperature N$_2$ adsorption, X-ray photoelectron spectroscopy, and transmission electron microscopy. It is shown that the sulfide catalysts prepared with glycols display higher activity in the hydrotreating of straight-run gas oil than the NiMoP/Al$_2$O$_3$ catalyst prepared without the additive. The hydrodesulfurization and hydrodenitrogenation activities depend on the glycol type and are decreased in the following order: NiMoP-DEG/Al$_2$O$_3$ > NiMoP-EG/Al$_2$O$_3$ > NiMoP-TEG/Al$_2$O$_3$ > NiMoP/Al$_2$O$_3$. The higher activity of NiMoP-DEG/Al$_2$O$_3$ can be explained with the higher dispersion of molybdenum on the surface of the catalyst in the sulfide state.

Keywords: hydrodesulfurization; phosphate-doped NiMo/Al$_2$O$_3$ catalyst; straight-run gas oil; XPS; ethylene glycol; diethylene glycol; triethylene glycol; hydrodenitrogenation

1. Introduction

Alumina-supported cobalt and nickel-promoted molybdenum sulfides are generally used in the refineries as hydrodesulfurization (HDS) catalysts to remove sulfur from petroleum fractions [1,2]. Increasingly stringent transportation fuel specifications and the necessity of refining of the new stocks, such as heavier crudes, shell oil, cracked stocks, and renewables, have stimulated the development of more active hydrotreating catalysts [3,4]. It is generally accepted that the active phase of hydrotreating catalysts is presented by layered nanoparticles of molybdenum disulfide decorated with cobalt or nickel atoms on the edge faces [2]. The dispersion of active metal, sulfidation degree, and amount of Co or Ni atoms on the edges of MoS$_2$ nanoparticles are the essential factors in the preparation of the so-called CoMoS or NiMoS active phase [1,2].

One of the recognized approaches to enhance the activity of HDS catalysts in the hydrotreating reactions is the addition of phosphoric acid to the impregnating solution [5–8]. Phosphate has a beneficial effect due to several factors, such as the increased solubility of the molybdenum salts, stability of the impregnation solution, and decreased metal-support interaction. Depending on the reaction conditions, phosphoric acid reacts with the molybdenum precursor (ammonium heptamolybdate or MoO_3) and gives a variety of phosphomolybdate anions, such as diphosphopentamolybdate ($P_2Mo_5O_{23}^{6-}$), Keggin ($PMo_{12}O_{40}^{3-}$), and Dawson ($P_2Mo_{18}O_{62}^{6-}$) heteropolyanions (HPAs). Further, the use of various types of organic modifiers during catalyst preparation has resulted in materials of enhanced HDS activity; both chelating agents and glycol-type additives are used for this purpose [1,3,4,6–12]. In contrast with ligand-type modifiers, such as α-hydroxycarboxylic, thioglycolic, or aminopolycarboxylic acid, only a limited number of publications have been found concerning the effect of glycol-type additives on catalytic properties of sulfide CoMo or NiMo catalysts [3,13].

Most articles describe the effect of glycols on the activity of CoMo systems, using post-treatment of $CoMo(P)/Al_2O_3$ systems with triethylene glycol (TEG) or polyethylene glycol (PEG) [14–16], or co-impregnation with the solution of active metals and glycols [6–9,17]. Just a few reports are found concerning the effect of addition of glycols to the impregnation solution on the activity of $NiMo/Al_2O_3$ catalysts [10–12]. It was shown that the glycol-modified catalysts displayed higher activity in the HDS of model compounds [6–12,16,17] and gasoil fractions [10,12,16,17], as well as in toluene hydrogenation [14,15]. Moreover, a synergetic effect of glycol-type additives and phosphate was disclosed [6,7,12]. It was proposed that glycols hinder the interaction between the active phase precursors and alumina, promoting the formation of sulfide phase with the improved activity [6,7,9–11]. However, the results concerning the effect of glycol addition on the dispersion of sulfide phase and surface distribution of promoter (Co, Ni) and Mo species (expressed as metal/alumina ratio) are rather contradictory. According to [9], dispersions of both Co and Mo are increased in the sulfide $CoMo(P)/Al_2O_3$ catalysts when ethylene glycol (EG), diethylene glycol (DEG), and TEG are added to impregnation solution. Using the results of the XPS study, the authors [12] came to the conclusion that the addition of PEG to the solution leads to the increase of Ni dispersion in the dried $NiMo(P)/Al_2O_3$ system, but has no effect on Mo distribution. The sulfide samples were not studied in this work. Using similar precursors and the XPS method for catalyst characterization, the authors [10] observed the decrease of Mo dispersion and increase of Ni dispersion in the $NiMo(P)/Al_2O_3$ sulfide catalysts after addition of TEG to impregnation solution. Besides, there is no information concerning the comparison of EG, DEG, and TEG effect on the catalytic properties of $NiMo/Al_2O_3$ catalyst. To the best of our knowledge, this effect was only studied for $CoMo(P)/Al_2O_3$ catalysts prepared starting from Keggin-type HPA in dibenzotiophene HDS [9].

In the present paper, we study the effect of various glycols on the activity of phosphate-doped $NiMo/Al_2O_3$ catalysts in the hydrotreating of straight-run gas oil (SRGO). The influence of EG, DEG, and TEG on Ni and Mo dispersion in the oxide (after drying at 110 °C) and sulfide (after liquid-phase sulfidation and HDS reaction) $NiMo(P)/Al_2O_3$ catalysts is also studied using XPS method.

2. Results and Discussion

2.1. Impregnation Solutions

The dissolution of MoO_3 in an aqueous solution of phosphoric acid for atomic ratio P/Mo = 0.4 (pH = 1.0) leads to a formation of Dawson-type heteropolyanion [5,18], according to Equation (1):

$$18MoO_3 + 2H_3PO_4 \rightarrow H_6P_2Mo_{18}O_{62}, \tag{1}$$
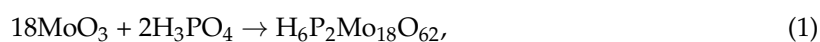
The Raman spectrum of this solution (denoted as MoP), containing major signals at 978, 955, 715, 648, 382, 242, 223, and 180 cm^{-1} (Figure 1), confirms the presence of Dawson entities [18,19].
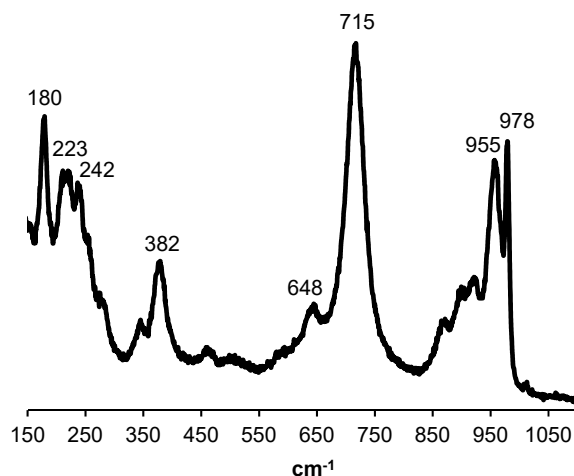
Figure 1. Raman spectrum of the MoP solution.

The HPA $H_xP_2Mo_{18}O_{62}^{(6-x)-}$ is decomposed upon addition of nickel hydroxide in the solution due to an increase of pH [5,18]. The Raman spectrum of obtained NiMoP solution (pH = 2.3) has peaks at 944, 892, 389, 370, and 216 cm^{-1}, characteristic of the presence of diphosphopentamolybdate anion $H_xP_2Mo_5O_{23}^{(6-x)-}$ (Figure 2a). The introduction of diethylene glycol to the NiMoP solution does not affect the bands of diphosphopentamolybdate anion. In addition to peaks of $H_xP_2Mo_5O_{23}^{(6-x)-}$, the spectrum of NiMoP-DEG solution has the small bands at 830 and 1060 cm^{-1} assigned to DEG vibrations (Figure 2b,c). The Raman spectra of the impregnation solutions containing EG and TEG were recorded as well and showed the same results (Figure S1).
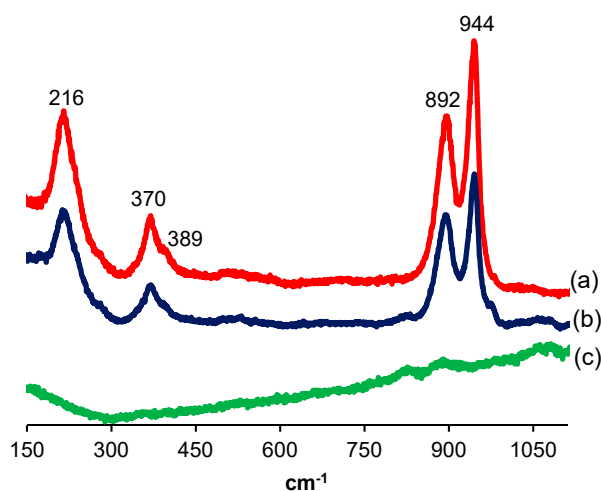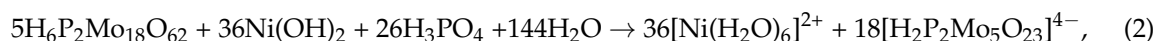

Figure 2. Raman spectra of aqueous solutions: (**a**) NiMoP, (**b**) NiMoP-DEG, and (**c**) DEG.

In order to determine nickel species presented in the NiMoP solution, UV–Vis absorption spectrum was recorded (Figure 3a). The broad band in the 550–800 nm region, with two maxima at about 650 and 720 nm, is assigned to the spin-allowed d–d transition $^3A_{2g} \rightarrow {}^3T_{1g}(F)$ of octahedrally coordinated nickel ions $[Ni(H_2O)_6]^{2+}$ [20]. This indicates that no nickel-diphosphopentamolybdate species are formed in the aqueous solution, as assumed in [6]. Therefore, the interaction of the MoP solution with nickel hydroxide can be presented formally by Equation (2):
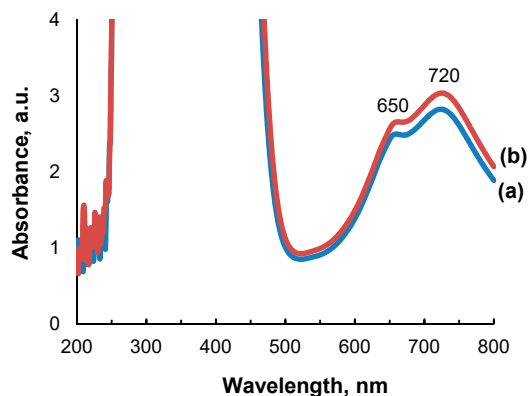
$$5H_6P_2Mo_{18}O_{62} + 36Ni(OH)_2 + 26H_3PO_4 + 144H_2O \rightarrow 36[Ni(H_2O)_6]^{2+} + 18[H_2P_2Mo_5O_{23}]^{4-}, \quad (2)$$

Figure 3. UV–Vis spectra of the solutions: (**a**) NiMoP and (**b**) NiMoP-DEG.

The UV–Vis spectrum of $[Ni(H_2O)_6]^{2+}$ cation is maintained in the presence of glycols (Figure 3b). Thus, we can conclude that the glycols do not interact with the metal precursors in the aqueous solution [6,10,11].

2.2. Catalyst Characterization

The phosphate-doped $NiMo/Al_2O_3$ catalysts were prepared by impregnation of γ-alumina granules with a subsequent drying at 110 °C for 4 h. The list and chemical composition of the prepared catalysts are presented in Table 1. The catalysts contained approximately the same amount of Mo with the Ni/Mo molar ratios of 0.4. The Raman spectra of dried samples are shown in Figure 4. All samples showed broad bands, which can be attributed to a mixed NiMo oxyhydroxide phase [18,21]. Meanwhile, the spectra do not contain the bands associated with HPA $H_xP_2Mo_5O_{23}^{(6−x)−}$. Therefore, when the impregnation solution comes in contact with the γ-Al_2O_3 surface, the diphosphopentamolybdate anion is decomposed completely. This is in accordance with literature data, in which it is stated that interaction of $H_xP_2Mo_5O_{23}^{(6−x)−}$ with the hydroxyl groups of the alumina results in the disintegration of the complex with the formation of amorphous $AlPO_4$ layer and molybdates [22,23].

Table 1. List and chemical composition of the catalysts [1].

Catalyst	Mo, wt%	Ni, wt%	P, wt%
NiMoP/Al_2O_3	13.4	3.4	2.0
NiMoP-EG/Al_2O_3	13.1	3.4	1.9
NiMoP-DEG/Al_2O_3	13.2	3.5	1.6
NiMoP-TEG/Al_2O_3	13.3	3.3	1.8

[1] The content of elements was determined by atomic absorption spectroscopy after calcination of the samples at 550 °C for 4 h.
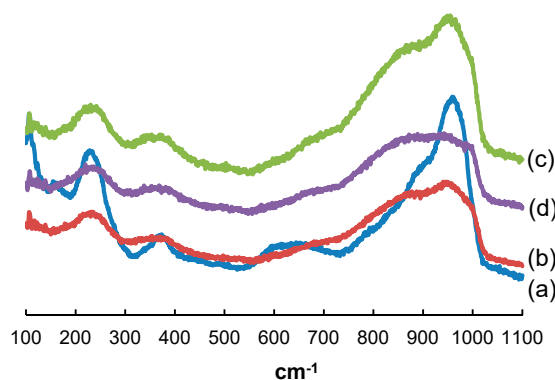

Figure 4. Raman spectra of dried solids: (**a**) NiMoP/Al_2O_3, (**b**) NiMoP-EG/Al_2O_3, (**c**) NiMoP-DEG/Al_2O_3, and (**d**) NiMoP-TEG/Al_2O_3.

The chemical surface composition of the catalysts in the oxide form was evaluated by XPS. The Mo3d spectrum of dried NiMoP/Al$_2$O$_3$ catalyst contains Mo3d$_{5/2}$ and Mo3d$_{3/2}$ doublet with a binding energy of 232.3 and 235.3 eV (Figure S2), which can be attributed to Mo^{6+} in oxide compound [9]. The spectra of other samples show slightly lower binding energies (231.9 and 234.9 eV) for Mo3d$_{5/2}$ and Mo3d$_{3/2}$ peaks. This can be explained by partial reduction of Mo^{6+} to Mo^{5+} during drying in the presence of glycol. The binding energy for Ni2p is 856.7 eV (Figure S3), which is characteristic of Ni^{2+} in nickel hydroxide [24,25]. Analysis of the recorded XPS spectra allowed estimating the Ni/Al and Mo/Al ratios. It is seen that addition of glycols to the impregnation solution has a minor effect on the Mo/Al ratio, but the Ni/Al ratio increases noticeably, from 0.044 to 0.051–0.065 (Table 2). Thus, the glycols provide the increase of Ni dispersion in the dried samples coinciding with the results obtained in [12].

Table 2. XPS data for phosphate-doped NiMo/Al$_2$O$_3$ catalysts.

Catalyst	Oxide Form		Sulfide Form	
	Ni/Al	Mo/Al	Ni/Al	Mo/Al
NiMoP/Al$_2$O$_3$	0.044	0.113	0.051	0.074
NiMoP-EG/Al$_2$O$_3$	0.051	0.112	0.041	0.141
NiMoP-DEG/Al$_2$O$_3$	0.065	0.123	0.056	0.151
NiMoP-TEG/Al$_2$O$_3$	0.063	0.120	0.040	0.116

The Mo3d spectra of the sulfide catalysts after testing in the hydrotreating of SRGO contain the Mo 3d$_{5/2}$ and 3d$_{3/2}$ doublet with binding energy at 228.9 and 232.1 eV (Figure 5 and Figure S4). The peak, with a binding energy of 226.3 eV, is assigned to S2s [9,10]. The data obtained from deconvolution of Mo3d and Ni2p spectra [26] are sufficiently similar for all catalysts (Table S1). The percentage of Mo atoms in different states is approximately the same in the different catalysts, being within the following limits of %: Mo^{4+}—75.8 ± 1.4; Mo^{5+}—14.2 ± 0.7; Mo^{6+}—10.0 ± 1.4. Consequently, the portion of Mo atoms in the MoS$_2$, as well as sulfidation degree, are similar for the studied catalysts. The evolution of Mo and Ni dispersion in terms of Mo/Al and Ni/Al ratios on the surface of the catalysts upon sulfidation is rather different. The Ni/Al ratio decreases in the EG, DEG, and TEG-modified catalysts after sulfidation, while this value increases for the NiMoP/Al$_2$O$_3$ sample (Table 2). The Mo/Al atomic ratio decreases on the surface of NiMoP/Al$_2$O$_3$ and NiMoP-TEG/Al$_2$O$_3$ catalysts, while sulfidation of NiMoP-EG/Al$_2$O$_3$ and NiMoP-DEG/Al$_2$O$_3$ leads to an increase in this ratio. Thus, the comparison of Ni/Al and Mo/Al ratios on the surface of NiMo(P)/Al$_2$O$_3$ catalysts in the oxide and sulfide state allows us to come to the conclusion that considerable redistribution of active metals occurs during sulfidation, and the nature of organic additive has a noticeable effect on this process. The Mo dispersion in the sulfide catalysts in the term of Mo/Al ratio is decreased in the following order: NiMoP-DEG/Al$_2$O$_3$ > NiMoP-EG/Al$_2$O$_3$ > NiMoP-TEG/Al$_2$O$_3$ > NiMoP/Al$_2$O$_3$.

The XRD patterns of the NiMo(P)/Al$_2$O$_3$ sulfide catalysts contain the characteristic diffraction peaks from γ-Al$_2$O$_3$ (PDF No. 29-0063) and MoS$_2$ (JCPDS No. 017-0744) phases (Figure S5). In all samples, the MoS$_2$ phase parameters slightly exceed the standard values (a = b = 3.162–3.163 Å, c = 18.371 Å, α = β = 90°, γ = 120°), apparently due to the incorporation of Ni atoms into molybdenum disulfide structure. The formation of nickel sulfide crystallites was not detected. The difference curves obtained by the subtraction of the XRD curve of the alumina from the catalyst showed two low-intensive broad diffraction peaks at 2θ = 33°–35° and 58°–60°, characteristic for the 100 and 110 planes of the MoS$_2$ hexagonal phase. The coherently scattering domains (D$_{XRD}$) were 4.0–4.5 nm (Table 3).

The TEM images of the NiMoP/Al$_2$O$_3$ and NiMoP-DEG/Al$_2$O$_3$ catalysts are presented in Figure 6; they are typical of NiMo/Al$_2$O$_3$ sulfide catalysts. The observed black thread-like fringes correspond to the structure of molybdenum disulfide MoS$_2$. The TEM images of the NiMoP-EG/Al$_2$O$_3$ and NiMoP-TEG/Al$_2$O$_3$ catalysts are very similar to the picture of NiMoP-DEG/Al$_2$O$_3$ sample. The average particle sizes determined by statistical processing of the TEM images are in the range

of 4.5–5.2 nm (Table 3). The average number of layers per particle is 1.9 for NiMoP/Al$_2$O$_3$; a slightly smaller value of stacking number in the sulfide nanoparticles (1.4–1.6) are obtained for the NiMoP-EG/Al$_2$O$_3$, NiMoP-DEG/Al$_2$O$_3$, and NiMoP-TEG/Al$_2$O$_3$ catalysts. These data correlate with the XPS results, which give higher Mo/Al ratios for glycol-modified catalysts. Thus, the TEM and XRD data give the evidence that the procedures used in catalyst preparation and sulfidation ensure the formation of dispersed NiMoS nanoparticles. The textural properties of all catalysts in the sulfide state did not differ significantly (Table 3).
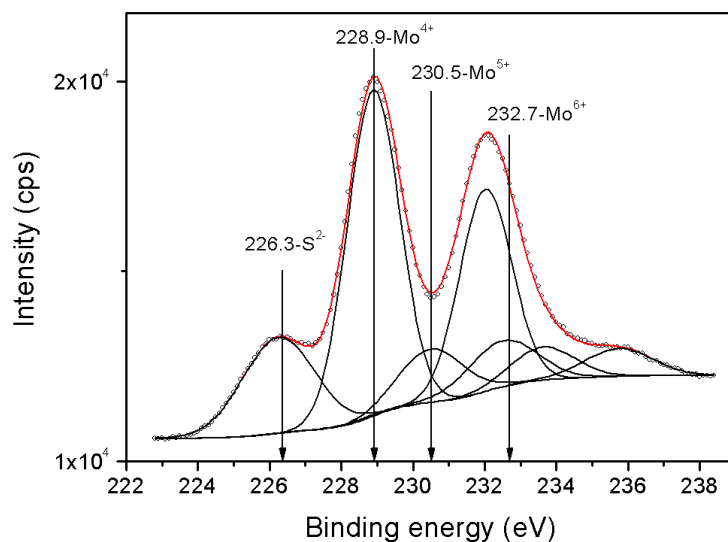

Figure 5. XPS Mo3d spectrum of the NiMoP-DEG/Al$_2$O$_3$ sulfide catalyst.

Table 3. Morphological and textural characteristics of the sulfide catalysts.

Catalyst	D_{XRD}, nm	Average Slab Length, nm	Stacking Number	S_{BET}, m^2 g^{-1}	V_{pore}, cm^3 g^{-1}	D_{pore}, nm
NiMoP/Al$_2$O$_3$	4.5	4.9	1.9	114	0.34	11.8
NiMoP-EG/Al$_2$O$_3$	4.0	4.7	1.4	120	0.36	11.9
NiMoP-DEG/Al$_2$O$_3$	4.4	5.2	1.6	129	0.34	10.7
NiMoP-TEG/Al$_2$O$_3$	4.1	4.5	1.5	127	0.35	10.9

(**a**)　　　　　　　　　　　　　　　　　　　　　　　　(**b**)
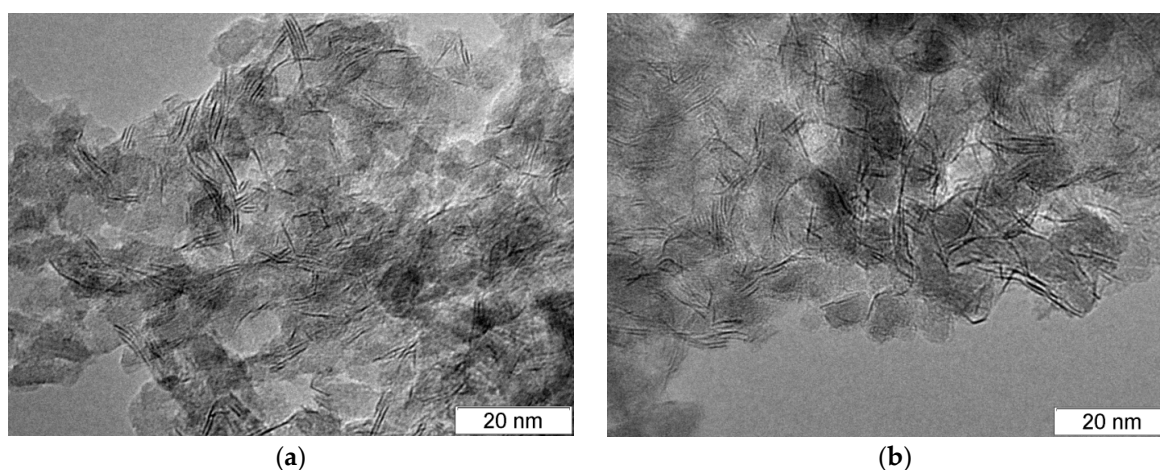
Figure 6. TEM image of sulfide catalyst: (**a**) NiMoP/Al$_2$O$_3$, (**b**) NiMoP-DEG/Al$_2$O$_3$.

2.3. Catalytic Activity

The catalytic properties of the NiMoP/Al$_2$O$_3$, NiMoP-EG/Al$_2$O$_3$, NiMoP-DEG/Al$_2$O$_3$, and NiMoP-TEG/Al$_2$O$_3$ catalysts were investigated in the hydrotreating of straight-run gas oil at

temperature of 330–340 °C, hydrogen pressure of 3.5 MPa, H_2/feedstock ratio of 300, and LHSV of 2 h^{-1}. The properties of the feedstock are listed in Table 4. The content of residual sulfur and nitrogen was determined for three samples taken 10, 11, and 12 h after the start of the experiment. According to the results obtained, the catalytic activity are not decreased during the reaction under the conditions used (Figures S6 and S7).

Table 4. Characteristics of the feedstock.

Property		Method
IBP [1]:0.5%V, °C	214.3	ASTM D2887
5%V, °C	243.5	
10%V, °C	250.7	
20%V, °C	259.3	
30%V, °C	266.8	
50%V, °C	282.9	
70%V, °C	303.4	
80%V, °C	315.5	
90%V, °C	330.9	
95%V, °C	343.2	
FBP [2]: 99.5%V, °C	349.4	
Sulfur content, ppm	8870	ASTM D 4294
Nitrogen content, ppm	110	ASTM D 4629
Total aromatics, wt%	28.0	IP 391
Monoaromatics, wt%	19.2	
Diaromatics, wt%	7.1	
Polyaromatics, wt%	1.7	
Density, g cm^{-3}	0.847	ASTM D 4052

[1] Initial boiling point; [2] Final boiling point.

The catalysts prepared using glycols show a higher HDS activity than the catalyst prepared without the additive (Table 5). This is consistent with the results obtained in [6–12]. The HDS activity decreased in the following order: NiMoP-DEG/Al_2O_3 > NiMoP-EG/Al_2O_3 > NiMoP-TEG/Al_2O_3 > NiMoP/Al_2O_3. The same effect is observed for the hydrodenitrogenation (HDN) of SRGO. A comparison of the hydrodesulfurization rate constants (k) calculated at 330 °C for NiMoP/Al_2O_3, NiMoP-EG/Al_2O_3, NiMoP-DEG/Al_2O_3, and NiMoP-TEG/Al_2O_3 catalysts demonstrates that the addition of EG, DEG, and TEG in the impregnation solution increases the catalytic activity by a factor of 2.2, 2.8, and 1.3, respectively. These results can be explained by the influence of organic additives on the dispersion of Mo in the sulfide catalyst (Table 2). Besides, the activity of NiMoP-DEG/Al_2O_3 exceeding that of NiMoP-EG/Al_2O_3 may be associated with a higher Ni dispersion (in terms of Ni/Al ratio).

Table 5. Catalytic properties of NiMo(P)/Al_2O_3 catalysts in the hydrotreating of SRGO [1].

Entry	Catalyst	T, °C	S, ppm	N, ppm	k, h^{-1} $ppm^{-0.6}$
1	NiMoP/Al_2O_3	330	340	19	0.031
2	NiMoP/Al_2O_3	340	166	15	–
3	NiMoP-EG/Al_2O_3	330	109	11	0.067
4	NiMoP-EG/Al_2O_3	340	60	6	–
5	NiMoP-DEG/Al_2O_3	330	74	4	0.086
6	NiMoP-DEG/Al_2O_3	340	34	3	–
7	NiMoP-TEG/Al_2O_3	330	246	16	0.039
8	NiMoP-TEG/Al_2O_3	340	142	12	–

[1] H_2 pressure of 3.5 MPa, H_2/feedstock of 300 Nm^3 m^{-3} and LHSV of 2 h^{-1}.

3. Materials and Methods

3.1. Catalyst Preparation

The support was γ-Al$_2$O$_3$ in the form of granules, with a trefoil-shaped cross section and a size of 1.2 mm (Promyshlennye Katalizatory Co., Ryazan, Russia). The textural properties of the carrier were BET surface area 235 m^2 g^{-1}, pore volume 0.79 cm^3 g^{-1}, average pore diameter 13.4 nm. Previously to impregnation, the support was dried at 110 $^\circ$C for 2 h. The catalysts were prepared by incipient wetness impregnation of γ-alumina granules with an aqueous solution containing the required amounts of precursors of active metals [6,10]. Chemicals were purchased from Acros Organics (Geel, Belgium) and Vekton (St. Petersburg, Russia) with $\geq$99% purity grade. Impregnation solutions were prepared as follows: MoO$_3$ (5.4 g, Vekton) and 85 wt% H$_3$PO$_4$ (1.0 mL, Vekton) were dissolved in water under stirring and refluxed at 80 $^\circ$C. When the MoO$_3$ was dissolved, 1.39 g of Ni(OH)$_2$ (Acros Organics) was added. At the next step, we added 1.6 mL of EG (Acros Organics), 2.75 mL of DEG (Acros Organics), and 3.9 mL of TEG (Acros Organics) for the preparation of the NiMoP-EG, NiMoP-DEG, and NiMoP-TEG solution, respectively. Molar concentrations of Mo, Ni, P, and glycol in impregnation solutions corresponded to 2.08 M, 0.83 M, 0.83 M, and 1.56 M, respectively. After impregnation, the samples were dried in nitrogen flow at room temperature and then at 110 $^\circ$C for 4 h. Reference material without an organic additive was also prepared.

3.2. Characterization Techniques

The Mo, Ni, and P content was measured by atomic absorption spectroscopy on an Optima 4300 DV instrument (Perkin Elmer, Waltham, MA, USA). The transmission electron microscopy (TEM) studies were performed by using a JEM-2010 (JEOL, Tokyo, Japan) electron microscope. The average size of the NiMoS nanoparticles was determined by counting over 350 particles in TEM images taken with medium magnification. Textural characteristics were determined from low temperature nitrogen adsorption isotherms obtained on a Micromeritics ASAP$^\circledR$ 2400 analyzer (Micromeritics, Norcross, GA, USA). UV–Vis spectra were recorded in the wavelength range of 200–800 nm using a Cary 60 UV-Vis Agilent spectrophotometer (Agilent Technologies, Santa Clara, CA, USA). Powder XRD patterns were obtained on a ARL X'TRA diffractometer (Thermo Fisher Scientific, Waltham, MA, USA) using CuK$_\alpha$ radiation. The measurements were performed in a range of 2θ from 5° to 70° with a scanning step of 0.05° and an accumulation time of 3 s per point. The JCPDS database was used in the phase analysis. The average crystallite sizes were defined using the Scherrer equation. The quantitative phase analysis and refining of the unit cell parameters were carried out by Rietveld analysis of a diffraction pattern using X'Pert High Score Plus software.

Raman measurements were carried out on a Raman spectrometer T64000 (Horiba Jobin Yvon, Kyoto, Japan). The spectra were recorded in the backscattering geometry at room temperature using Ar$^+$ laser for excitation; wavelength is 514.5 nm. Incident light was linearly polarized. The spectral resolution was not worse than 2 cm^{-1}. The silicon CCD matrix was used as photodetector; it was cooled with liquid nitrogen. An attachment based on an Olympus microscope was used for microscopic analysis of the Raman spectra. The power of the laser beam at the sample was about 2 mW. To avoid heating the structures by laser beam, the sample was placed slightly further than the focus, so the spot size was 20 μm.

X-ray photoelectron spectra (XPS) were recorded on a SPECS (SPECS GmbH, Berlin, Germany) photoelectron spectrometer using a hemispherical PHOIBOS-150-MCD-9 analyzer (non-monochromatic Al Kα radiation, hν = 1486.6 eV, 200 W). The binding energy (BE) scale was pre-calibrated using the positions of the peaks of Au4f$_{7/2}$ (BE = 84.0 eV) and Cu2p$_{3/2}$ (BE = 932.67 eV) core levels. The samples in the form of a powder were loaded onto a conducting double-sided copper scotch. The Al2p peak (BE = 74.5 eV) corresponding to Al^{3+} from Al$_2$O$_3$ support was used as an internal reference [27]. The atomic concentration ratios of elements on the catalyst surface were calculated from the integral photoelectron peak intensities (Al2p, Mo3d and Ni2p), which were corrected with theoretical sensitivity factors based

on the Scofield's photo-ionization cross sections [28]. The differences in the binding energies for each catalyst did not exceed 0.1 eV.

3.3. Catalytic Activity Test

The catalysts were tested in a flow reactor with an inner diameter of 16 mm and length of 570 mm, as described in [29]. The reactor was loaded with catalyst granules (granule length of 4–5 mm, total volume of 10 mL) diluted with an inert material, carborundum (grain size of 0.10–0.25 mm), in a volume ratio of 1:2. The catalyst was sulfided in situ prior to the experiment with straight-run gas oil, additionally containing 0.6 wt% sulfur as dimethyl disulfide (H_2 pressure of 3.5 MPa; H_2/feedstock of 300 Nm^3/m^3; liquid hourly space velocity of 2 h^{-1}). The sulfidation was performed in two steps, the first one at 240 °C for 8 h and the second at 340 °C for 6 h. The straight-run gas oil (from Urals crude oil) was used as the feedstock (Table 4). The catalytic experiments were performed at temperature of 330–340 °C, hydrogen pressure of 3.5 MPa, H_2/feedstock ratio of 300 Nm^3 hydrogen m^{-3} feedstock, and liquid hourly space velocity of 2 h^{-1}. The duration of each stage differing in condition was 12 h; the residual S and N content was obtained by averaging the data for three samples taken through 10, 11, and 12 h after the beginning of the current stage. The sulfur content in the feedstock and hydrogenated products was measured on a Lab-X 3500SCl energy dispersive X-ray fluorescence analyzer (Oxford Instruments, Abingdon, UK) and on an ANTEK 9000NS analyzer (for products containing less than 100 ppm S). The nitrogen content was determined using an ANTEK 9000NS (Antek, Houston, TX, USA). To perform XPS and TEM analysis, the sulfide catalyst after testing in the hydrotreating of SRGO was dumped out from the reactor and then washed by hexane. To remove hexane, the sample was placed in the vacuum heat chamber at room temperature, evacuated to 5 mbar, and dried at this temperature for 15 h.

To measure HDS activity, the reaction rate constant (k) was calculated using Equation (3):

$$\frac{k(n-1)}{W} = \frac{1}{[S]^{n-1}} - \frac{1}{[S_0]^{n-1}}, \tag{3}$$

where W is the liquid hourly space velocity ((m^3 feedstock) (m^3 catalyst)$^{-1}$ h^{-1}), [S] and [S_0] are the sulfur contents of the hydrogenated products and feedstock (wt%), respectively, and $n = 1.6$ [29].

4. Conclusions

The effect of ethylene glycol (EG), diethylene glycol (DEG), and triethylene glycol (TEG) on the properties of phosphate-doped $NiMo/Al_2O_3$ hydrotreating catalysts has been investigated. The addition of glycols to the impregnation solution prepared by the dissolving of MoO_3, H_3PO_4, and $Ni(OH)_2$ in water leads to the increased dispersion of Mo on the surface of sulfide catalysts, in terms of Mo/Al ratio. Both Mo dispersion in the terms of Mo/Al ratio and HDS and HDN activity of catalysts in SRGO hydrotreating are decreased in the following order: $NiMoP-DEG/Al_2O_3$ > $NiMoP-EG/Al_2O_3$ > $NiMoP-TEG/Al_2O_3$ > $NiMoP/Al_2O_3$. Consequently, the beneficial effect of glycols on the HDS and HDN activity can be explained by the improved dispersion of Mo on the surface of sulfide catalysts prepared with the glycol-type additives. The highest dispersion of Mo and activity were shown by the catalyst with DEG, which is 2.8 times more active in the HDS of straight-run gas oil than a similar catalyst prepared without additive. Comparing the Ni/Al and Mo/Al ratios on the surface of $NiMo(P)/Al_2O_3$ catalysts in the oxide and sulfide state allows us to conclude that a considerable redistribution of active metals takes place during sulfidation. Moreover, the nature of organic additive has a noticeable effect on this process. To get a deeper insight into the effect of the glycol nature on the dispersion of sulfide nanoparticles and catalytic properties, a thorough study of sulfidation mechanism should be performed using H_2S or dimethyldisulfide as the sulfiding agent.

Supplementary Materials: The following are available online at http://www.mdpi.com/2073-4344/9/1/96/s1: Figure S1: Raman spectrum of NiMoP-TEG solution; Figure S2: XPS Mo3d spectra of the catalysts in oxide form:

(a) NiMoP/Al$_2$O$_3$, (b) NiMoP-EG/Al$_2$O$_3$, (c) NiMoP-DEG/Al$_2$O$_3$, and (d) NiMoP-TEG/Al$_2$O$_3$; Figure S3: XPS Ni2p spectra of the catalysts in oxide form: (a) NiMoP/Al$_2$O$_3$, (b) NiMoP-EG/Al$_2$O$_3$, (c) NiMoP-DEG/Al$_2$O$_3$, and (d) NiMoP-TEG/Al$_2$O$_3$; Figure S4: XPS Mo3d and S2s spectra of the catalysts in sulfide state: (a) NiMoP/Al$_2$O$_3$, (b) NiMoP-EG/Al$_2$O$_3$, (c) NiMoP-DEG/Al$_2$O$_3$, and (d) NiMoP-TEG/Al$_2$O$_3$; Figure S5: XRD patterns of the NiMoP-DEG/Al$_2$O$_3$ sulfide catalyst; Figure S6: Catalytic properties of NiMo(P)/Al$_2$O$_3$ catalysts in hydrodesulfurization of SRGO: (a) 330 °C and (b) 340 °C; Figure S7: Catalytic properties of NiMo(P)/Al$_2$O$_3$ catalysts in hydrodenitrogenation of SRGO: (a) 330 °C and (b) 340 °C; Figure S8: XPS Ni2p spectra of the catalysts in sulfide state: (a) NiMoP/Al$_2$O$_3$, (b) NiMoP-EG/Al$_2$O$_3$, (c) NiMoP-DEG/Al$_2$O$_3$, and (d) NiMoP-TEG/Al$_2$O$_3$; Figure S9: Deconvolution of Ni2p spectrum of the NiMoP-DEG/Al$_2$O$_3$ sulfide catalyst; Table S1: Molybdenum and nickel surface species of phosphate-doped NiMo/Al$_2$O$_3$ sulfide catalysts, as determined by XPS analysis.

References

1. Topsøe, H.; Clausen, B.S.; Massoth, F.E. *Hydrotreating Catalysis Science and Technology*; Springer: New York, NY, USA, 1996; ISBN 3-540-60380-8.
2. Pecoraro, T.A.; Chianelli, R.R. Hydrodesulfurization catalysis by transition metal sulfides. *J. Catal.* **1981**, *67*, 430–445. [CrossRef]
3. Stanislaus, A.; Marafi, A.; Rana, M.S. Recent advances in the science and technology of ultra-low sulfur diesel (ULSD) production. *Catal. Today* **2010**, *153*, 1–68. [CrossRef]
4. Ito, E.; van Veen, J.A.R. On novel processes for removing sulphur from refinery streams. *Catal. Today* **2006**, *116*, 446–460. [CrossRef]
5. Griboval, A.; Blanchard, P.; Payen, E.; Fournier, M.; Dubois, J.L. Alumina supported HDS catalysts prepared by impregnation with new heteropolycompounds. Comparison with catalysts prepared by conventional Co-Mo-P coimpregnation. *Catal. Today* **1998**, *45*, 277–283. [CrossRef]
6. Nicosia, D.; Prins, R. The effect of glycol on phosphate-doped CoMo/Al$_2$O$_3$ hydrotreating catalysts. *J. Catal.* **2005**, *229*, 424–438. [CrossRef]
7. Nicosia, D.; Prins, R. The effect of phosphate and glycol on the sulfidation mechanism of CoMo/Al$_2$O$_3$ hydrotreating catalysts: An in situ QEXAFS study. *J. Catal.* **2005**, *231*, 259–268. [CrossRef]
8. Van Haandel, L.; Bremmer, G.M.; Hensen, E.J.M.; Weber, T. The effect of organic additives and phosphoric acid on sulfidation and activity of (Co)Mo/Al$_2$O$_3$ hydrodesulfurization catalysts. *J. Catal.* **2017**, *351*, 95–106. [CrossRef]
9. Pimerzin, A.; Mozhaev, A.; Varakin, A.; Maslakov, K.; Nikulshin, P. Comparison of citric acid and glycol effects on the state of active phase species and catalytic properties of CoPMo/Al$_2$O$_3$ hydrotreating catalysts. *Appl. Catal. B Environ.* **2017**, *205*, 93–103. [CrossRef]
10. Escobar, J.; Barrera, M.C.; Toledo, J.A.; Cortes-Jacome, M.A.; Angeles-Chavez, C.; Nunez, S.; Santes, V.; Gomez, E.; Dıaz, L.; Romero, E.; et al. Effect of ethyleneglycol addition on the properties of P-doped NiMo/Al$_2$O$_3$ HDS catalysts: Part I. Materials preparation and characterization. *Appl. Catal. B Environ.* **2009**, *88*, 564–575. [CrossRef]
11. Gutiérrez-Alejandre, A.; Laurrabaquio-Rosas, G.; Ramírez, J.; Busca, G. On the role of triethyleneglycol in the preparation of highly active Ni-Mo/Al$_2$O$_3$ hydrodesulfurization catalysts: A spectroscopic study. *Appl. Catal. B Environ.* **2015**, *166–167*, 560–567. [CrossRef]
12. Iwamoto, R.; Kagami, N.; Sakoda, Y.; Iino, A. Effect of polyethylene glycol addition on NiO-MoO$_3$/Al$_2$O$_3$ and NiO-MoO$_3$-P$_2$O$_5$/Al$_2$O$_3$ hydrodesulfurization catalyst. *J. Jpn. Petrol. Inst.* **2005**, *48*, 351–357. [CrossRef]
13. Rob van Veen, J.A. What's new? On the development of sulphidic HT catalysts before the molecular aspects. *Catal. Today* **2017**, *292*, 2–25. [CrossRef]
14. Costa, V.; Marchand, K.; Digne, M.; Geantet, C. New insights into the role of glycol-based additives in the improvement of hydrotreatment catalyst performances. *Catal. Today* **2008**, *130*, 69–74. [CrossRef]

15. Costa, V.; Guichard, B.; Digne, M.; Legens, C.; Lecour, P.; Marchand, K.; Raybaud, P.; Krebs, E.; Geantet, C. A rational interpretation of improved catalytic performances of additive-impregnated dried CoMo hydrotreating catalysts: A combined theoretical and experimental study. *Catal. Sci. Technol.* **2013**, *3*, 140–151. [CrossRef]

16. Nguyen, T.S.; Loridant, S.; Chantal, L.; Cholley, T.; Geantet, C. Effect of glycol on the formation of active species and sulfidation mechanism of CoMoP/Al₂O₃ hydrotreating catalysts. *Appl. Catal. B Environ.* **2011**, *107*, 59–67. [CrossRef]

17. Iwamoto, R.; Kagami, N.; Iino, A. Effect of polyethylene glycol addition on hydrodesulfurization activity over CoO-MoO₃/Al₂O₃ catalyst. *J. Jpn. Petrol. Inst.* **2005**, *48*, 237–242. [CrossRef]

18. Blanchard, P.; Lamonier, C.; Griboval, A.; Payen, E. New insight in the preparation of alumina supported hydrotreatment oxidic precursors: A molecular approach. *Appl. Catal. A Gen.* **2007**, *322*, 33–45. [CrossRef]

19. Briand, L.E.; Valle, G.M.; Thomas, H.J. Stability of the phospho-molybdic Dawson-type ion $P_2Mo_{18}O_{62}{}^{6-}$ in aqueous media. *J. Mater. Chem.* **2002**, *12*, 299–304. [CrossRef]

20. Klimova, T.E.; Valencia, D.; Mendoza-Nieto, J.A.; Hernandez-Hipolito, P. Behavior of NiMo/SBA-15 catalysts prepared with citric acid in simultaneous hydrodesulfurization of dibenzothiophene and 4,6-dimethyldibenzothiophene. *J. Catal.* **2013**, *304*, 29–46. [CrossRef]

21. Payen, E.; Grimblot, J.; Kasztelan, S. Study of oxidic and reduced alumina-supported molybdate and heptamolybdate species by in situ laser Raman spectroscopy. *J. Phys. Chem.* **1987**, *91*, 6642–6648. [CrossRef]

22. Bergwerff, J.A.; Visser, T.; Leliveld, B.R.G.; Rossenaar, B.D.; de Jong, K.P.; Weckhuysen, B.M. Envisaging the physicochemical processes during the preparation of supported catalysts: Raman microscopy on the impregnation of Mo onto Al₂O₃ extrudates. *J. Am. Chem. Soc.* **2004**, *126*, 14548–14556. [CrossRef] [PubMed]

23. Van Veen, J.A.R.; Hendriks, P.A.J.M.; Andrea, R.R.; Romers, E.J.G.M.; Wilson, A.E. Chemistry of phosphomolybdate adsorption on alumina surfaces. 2. The molybdate/phosphated alumina and phosphomolybdate/alumina systems. *J. Phys. Chem.* **1990**, *94*, 5282–5285. [CrossRef]

24. Ahn, K.-S.; Nah, Y.-C.; Sung, Y.-E. Surface morphological, microstructural, and electrochromic properties of short-range ordered and crystalline nickel oxide thin films. *Appl. Surf. Sci.* **2002**, *199*, 259–269. [CrossRef]

25. Biesinger, M.C.; Paine, B.P.; Lau, A.; Gerson, L.W.M.; Smart, R.St.C. X-ray photoelectron spectroscopic chemical state quantification of mixed nickel metal, oxide and hydroxide systems. *Surf. Interface Anal.* **2009**, *41*, 324–332. [CrossRef]

26. Klimov, O.V.; Leonova, K.A.; Koryakina, G.I.; Gerasimov, E.Yu.; Prosvirin, I.P.; Cherepanova, S.V.; Budukva, S.V.; Pereyma, V.Yu.; Dik, P.P.; Parakhin, O.A.; et al. Supported on alumina Co-Mo hydrotreating catalysts: Dependence of catalytic and strength characteristics on the initial AlOOH particle morphology. *Catal. Today* **2014**, *220–222*, 66–77. [CrossRef]

27. Moulder, J.F.; Stickle, W.F.; Sobol, P.E.; Bomben, K.D. *Handbook of X-ray Photoelectron Spectroscopy*; Chastain, J., Ed.; Perkin-Elmer: Eden Prairie, MN, USA, 1992; p. 261. ISBN 0962702625.

28. Scofield, J.H. Hartree-Slater subshell photoionization cross-sections at 1254 and 1487 eV. *J. Electron Spectrosc. Relat. Phenom.* **1976**, *8*, 129–137. [CrossRef]

29. Vlasova, E.N.; Deliy, I.V.; Nuzhdin, A.L.; Aleksandrov, P.V.; Gerasimov, E.Yu.; Aleshina, G.I.; Bukhtiyarova, G.A. Catalytic properties of CoMo/Al₂O₃ sulfide catalysts in the hydrorefining of straight-run diesel fraction mixed with rapeseed oil. *Kinet. Catal.* **2014**, *55*, 481–491. [CrossRef]